INTERFACE CAPTURING SIMULATIONS ON POOL BOILING PERFORMANCE WITH MULTIPLE NUCLEATION SITES

Yuqiao Fan[a], Mengnan Li[b], William D. Pointer[c], and Igor A. Bolotnov[a]

[a]Department of Nuclear Engineering
North Carolina State University
2500 Stinson Drive, Raleigh, NC 27607, USA

[b]School of Earth Science
Ohio State University
125 Oval Dr S, Columbus, OH 43210, USA

[c]Advanced Reactor Engineering and Development
Oak Ridge National Laboratory
1 Bethel Valley Rd, Oak Ridge, TN 37831, USA

yfan11@ncsu.edu; li.5382@osu.edu; pointerwd@ornl.gov; igor_bolotnov@ncsu.edu

ABSTRACT

High-fidelity pool boiling simulations can provide a numerical database for improving mechanistic boiling models by allowing for specific evaluation of interactions among bubbles. Previously published pool boiling simulations investigated two nucleation sites in which bubble growth at one site suppressed nucleation at the other site. Based on previous study results, more complicated interface-capturing simulations on pool boiling were conducted using PHASTA code with locally refined unstructured mesh.

First, different boundary conditions (BCs) were assessed to support robustness and reproducibility of the boiling model. Then, a scale study was conducted at a larger domain with nine nucleation sites, four of which were activated. Involving more nucleation sites increased the complexity of bubble interactions from surrounding sites. Finally, bubble departure behavior influenced by wall heat flux was investigated. When heat flux was increased, the order of bubble departure changed, but diagonal bubbles always departed after one another. The departure time interval between the first and second bubble reduced as heat flux increased. The corresponding frequency was almost linearly proportional to the heat flux. In addition, bubble departure behavior was found to be greatly influenced by the nucleation site pattern. Multiple nucleation sites resulted in superimposed inhibitive effects from surrounding sites to each bubble, which extensively delayed the departure.

The work presented here provides new insight on the fundamental understanding of boiling phenomena, contributes to the development of a 3D multiphase computational fluid dynamics (M-CFD) model, and provides a more comprehensive database for data-driven pool boiling studies.

KEYWORDS
pool boiling, nucleation site interaction, high-fidelity simulation, level-set method

1. INTRODUCTION

Boiling has proved to be one of the most efficient means for heat transfer and is widely used for heat removal in light-water reactors (LWRs), particularly when the coolant is being heated by the fuel rods during severe accident scenarios after reactor scram. Ideally, the remaining heat would be removed through boiling to mitigate the risk of reactor meltdown. The boiling process usually starts with natural convection boiling. As heat flux or wall temperature increases, nucleate boiling occurs when bubbles form on the heated surface and then depart. As heat flux increases further, bubbles form a vapor film on the heated surface which prevents the liquid from cooling the rod's surface. This phenomenon is referred to as *departure from nucleate boiling* (DNB), and the corresponding heat flux, which limits the heat transfer coefficient, is the *critical heat flux* (CHF). Experimental studies on high heat flux boiling are plentiful, but the topic is challenging for advanced modeling and simulations. In this case, high-fidelity pool boiling simulations can provide a numerical database for improving mechanistic boiling models, and the interactions among bubbles can be evaluated.

The distance between neighboring nucleation sites (S) determines how bubble growth at one site affects the boiling process at the adjacent site. Such nucleation site interactions have significant effects on boiling characteristics such as bubble departure frequency and diameter [1-3]. Regarding bubble departure diameter D_d, Chekanov [4] proposed a dimensionless distance S/D_d to categorize the bubble interactions effect. If S/D_d <1, then bubble growth will be promoted because of the effects of the adjacent bubble. When $S/D_d \in (1,3)$, then it is in the *inhibitive region*, in which bubble growth at one site suppresses the nucleation at the other site. $S/D_d > 3$ is considered the *independent region*, in which one bubble has a negligible effect on the growth and departure of the other bubble.

Previously published pool boiling simulations studied two nucleation sites [5]. However, when more nucleation sites are involved, the complexity of bubble suppression from surrounding sites increases, as well. To improve the understanding of bubble departure behavior, additional interface capturing simulations are needed on pool boiling scenarios with multiple nucleation sites. Furthermore, larger scale simulations are needed to further test the boiling solver capability. In addition, previous publications used a relatively low heat flux ($q" = 50 W/m^2$) for all pool boiling simulations [5,6] and may not be directly applicable in high heat flux boiling scenarios of LWRs. To move towards such heat flux conditions, the simulated heat flux must be increased by orders of magnitude.

The remainder of this paper is structured as follows. Section 2 briefly introduces the numerical methods, including the boiling model in PHASTA code, as well as the level-set method, which is the interface capturing approach implemented in PHASTA for two-phase simulations. Section 3 presents three boiling studies: (1) assessment of robustness and reproducibility of the boiling model via two nucleation site boiling simulations, (2) a scale test with a large domain having 9 nucleation sites, 4 of which were activated, and (3) bubble departure and interaction studies under various heat fluxes. The objective of these three studies is to fill in the critical gap in capability development, providing new insights on the fundamental understanding of boiling phenomena, contributing to the development of a 3D multiphase computational fluid dynamics (M-CFD) model, and providing a more comprehensive database for data-driven pool boiling studies.

2. NUMERICAL METHODS

PHASTA (Parallel, Hierarchic, higher-order accurate, Adaptive, Stabilized, finite element method Transient Analysis) was used to conduct the pool boiling studies presented herein [7,8]. PHASTA uses the level-set method, coupled with the finite element-based Navier-Stokes flow solver, which can achieve accurate solutions in simple and complex geometries [9,10].

Under the Consortium for the Advanced Simulation of Light Water Reactors (CASL), a boiling model was implemented in PHASTA to study boiling phenomena with high-resolution interface-resolved simulations. Such high-fidelity boiling simulations have become more affordable with the advancement of high-performance computing (HPC). Many research efforts have focused on development of the boiling model in PHASTA, including sub-grid contact angle models, flow boiling validation, and bubble boiling simulations with two nucleation sites [5,6,11]. This section briefly introduces the governing equations in PHASTA, the level-set method, and the boiling model.

2.1. Governing Equations

The incompressible flow solver was used in the simulations presented below. Incompressible Navier-Stokes (INS) equations for mass and momentum conservation, as well as conservation of energy, were used in the boiling solver of PHASTA:

$$\nabla \cdot \vec{u} = 0 \tag{1}$$

$$\rho \left[\frac{\partial \vec{u}}{\partial t} + (\vec{u} \cdot \nabla)\vec{u}\right] = -\nabla p + \mu \nabla^2 \vec{u} + \rho f \tag{2}$$

$$\rho c_p \left[\frac{\partial T}{\partial t} + (\vec{u} \cdot \nabla) T\right] = \nabla \cdot (k \nabla T) + q \tag{3}$$

In mass and momentum conservation Eqs. (1) and (2), $\vec{u}$ is the velocity, ρ and μ are the density and viscosity based on the local fluid phase, ∇p is the pressure gradient, $\mu \nabla^2 \vec{u}$ is the viscous stress tensor, and
ρf is the body force. In energy conservation Eq. (3), c_p is the specific heat, T is the absolute temperature of the fluid, and k is the thermal conductivity. Note that q represents heat generated by friction and is thus neglected in low viscous fluid such as water.

2.2. Level-set method

The level-set method has been used in two-phase studies and was incorporated in PHASTA to solve the INS equations for two-phase flow [12-14].This method uses a level set function, φ, to distinguish each phase (negative in gases, positive in liquids, zero at the interface), and the magnitude of φ is the shortest distance to the interface. Coupling with the fluid equations, the interface, defined where $\varphi = 0$, is advected first followed by a re-distancing process to re-establish the φ distribution near the interface both in the gas and liquid phases. Without re-distancing, $|\nabla\varphi|$ near $\varphi = 0$ can become very large or very small, which increases numerical error in level-set and even velocity.

2.3. Boiling model

The boiling model in PHASTA is activated at each time step. Bubble growth during boiling is achieved through three major steps [6]: (1) the local temperature gradient of each bubble is collected through the bubble tracking capability in PHASTA, (2) the heat flux across the interface is averaged for each bubble, which is then converted to volume change, and (3) the volume change is implemented by adding a volumetric source term in the mass continuity equation. By moving the interface outward uniformly, volume can be added inside the bubble.

3. SIMULATIONS AND RESULTS

The boiling simulations presented in this section were used to study pool boiling phenomena with multiple nucleation sites. Section 3.1 assesses the BC effect on the robustness and reproducibility of the boiling solver with two nucleation sites. Section 3.2 describes a scale test with a larger domain having 9 nucleation sites, 4 of which were activated. Bubble departure and interaction studies were conducted with increasing heat flux in Section 3.3. This represents a significant improvement over previous pool boiling simulations with low heat flux. At last, the bubble departure time and diameters are compared and analyzed under different nucleation site patterns in Section 3.4.

3.1. Pool Boiling Simulation on Two Nucleation Sites

This section describes the boiling simulations for two nucleation sites applying different boundary conditions. Different types of boundary condition leads to changes in physical interpretation of the nucleation site distribution, which further affects the bubble departure time and diameters in boiling simulations. The reference pool boiling case specifies a 4 mm distance between two sites and a heat flux of $q'' = 50\ W/m^2$ [5]. To assess the robustness and reproducibility of the boiling model, the BC presented in this section varied from the previous wall BC to symmetric and periodic BCs. Because the boiling solver could handle a wide range of BCs, the scale test and studies on heat flux effect could be carried out.

3.1.1. Reference case

For the reference boiling simulation, the domain with two nucleation sites is illustrated in Figure 1 (a). Two nucleation sites were prescribed as cavities at the bottom of the domain. The geometry of the cavities was selected to be a flat cylinder with a diameter of 1 mm and a depth of 0.1 mm. Two bubbles were initialized
at the top of the cavity with diameters of 1.12 mm. Since the contact angle algorithm was only activated on the heated surface, the bubble diameter should be slightly larger than the cavity size. Therefore, during the bubble growth the surface expanded on the heated surface rather than the cavity surface. Correspondingly, the contact angle force could drive the interface to form the correct angle with the heated wall. After bubble departure, the cavity with the depth allowed the remaining liquid to continue the evaporation process for the next boiling cycle. Other cavity shapes can also be used since cavity was not a defining factor in the boiling process. The bubble growth depends on the heat flux collected across the interface, rather than from the cavities. The distance between the two cavities was 4 mm. The bottom wall was assigned with a heat flux of $q'' = 50\ W/m^2$, and the top face had a pressure outlet BC. On the front and back walls (Face 81 and 85), periodic BCs were assigned. However, the remaining two surfaces (left and right walls, Faces 216 and 267) that used wall BCs as constant liquid inlet velocities were designated at the two vents to avoid backflow from the outlet. Those two surfaces will be changed into symmetric and periodic BCs to ensure robustness and reproducibility in future tests.

Figure 1 (b) depicts the spatial discretization of the computation domain using tetrahedral elements generated by meshing libraries of Simmetrix. The bubble is shown inside the most refined region, with 19 elements across the diameter. The remaining domain was discretized, with element resolutions increased by a factor of 2. The total mesh size was 1.9 M, and it took 2,814 core-hours to observe the first bubble departure on the local cluster *Insight*. The bubble departure diameter was $D_d = 3.6\ mm$. The simulation using this geometry and mesh setting was successfully conducted using wall BCs on the left and right faces of the computation domain [5]. Periodic and symmetric BCs were not applied due to numerical challenges. More details about boundary treatment in boiling simulations will be discussed in Section 3.1.3.

The nucleation site distribution on the bottom surface in the domain of Figure 1 (a) is depicted in Figure 2 (a). With BCs on faces 216 and 267 changed from wall to symmetric BCs, the new physical interpretation of the nucleation site distribution is that nearby sites are involved, as shown in Figure 2 (b). With wall BC changed to periodic BC, the physical interpretation of the site distribution becomes an infinite long domain

with a row of nucleation sites, as shown in Figure 2 (c). The major difference between the reference case and Figure 2 (b)/(c) is the appearance of the wall. As for the difference between (b) and (c), under symmetric BC, the liquid behavior in the vicinities of left and right boundary faces were independent of each, other considering a 10 mm distance in between. However, under periodic BC, the local fluid mechanics near two boundary faces affected each other, which might yield more complicated bubble-liquid interactions. The BC was changed to test the robustness and reproducibility of the boiling solver results. The key simulation parameters are summarized in Table I.

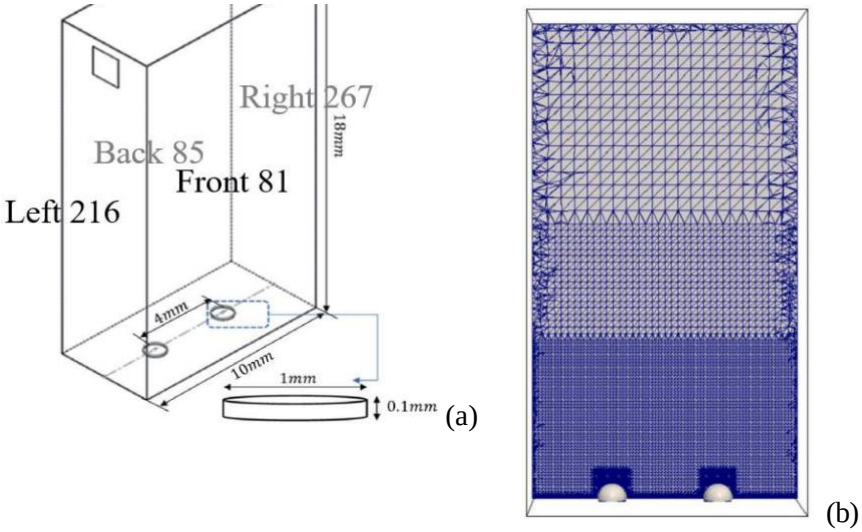

Figure 1. Computation domain (adapted from Fig.4 of Li et al. [5], with permission)

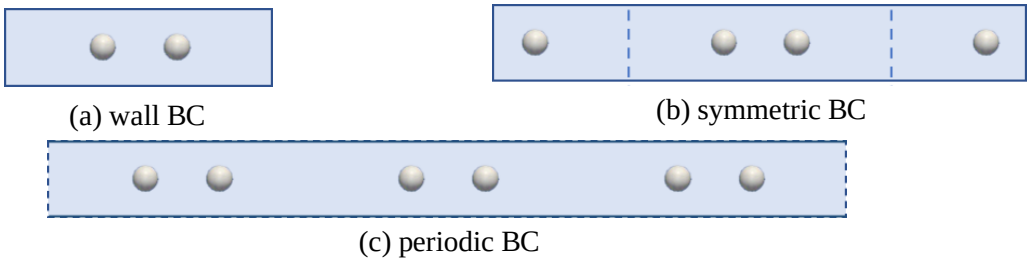

Figure 2. Physical interpretations of bubble distributions under different BCs of face 216 and 267

Table I. Key Parameters of Boiling Simulations.

Item	Liquid	Vapor
Viscosity ($Pa \cdot s$)	8.514E-04	1.858E-4
Density (kg/m^3)	958.0	0.579
Specific heat ($J/kg \cdot K$)	4.218e3	2.034e3
Thermal conductivity ($W/m \cdot K$)	0.679	0.025
Prandtl Number	1.75	
Surface Tension (N/m)	0.0625	
Latent heat (J/kg)	2260.0E3	
Contact angle (degree)	30.0	
Heat flux (W/m^2)	50.0	

In Table I, the contact angle was chosen to be a small value based on the surface condition and fluid properties in the boiling phenomenon in light water reactor subchannels. The corresponding bubble departure time and diameter were also small, and a low wall superheat was needed for the onset of nucleate boiling [15]. Therefore, a superheat of only $3°C$ (initialized as the bottom wall) was adequate, which can relieve some computational burden. The temperature field across the domain was initialized as a linear function, with $103°C$ at the bottom wall and $90°C$ at the top wall.

3.1.2. Symmetric BC

The simulation of two-bubble boiling with symmetric BC on the left and right surfaces was carried out, and Figure 3 shows how the departed bubbles coalesced with each other. *Scr2* is the bubble ID, which is a parameter in PHASTA representing each individual bubble. Bubble IDs are all integers starting from 1. During the boiling process, after bubble departure, the bubble ID was reassigned when the total number of bubbles changed. The computation time at coalescence was 64.63 ms, which is almost equal to that in the reference case under the wall BC on the left and right surfaces (64.90 ms) [5]. Since the liquid near the two walls was almost stagnant, the appearance of the wall had negligible effect on the bubble departure. Therefore, changing from wall to symmetric BC should not affect coalescence time.

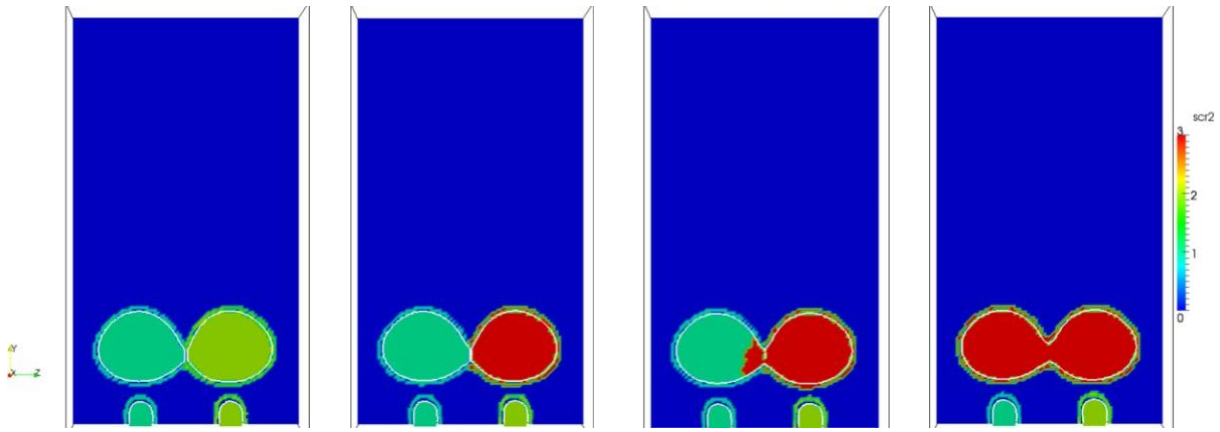

(a) 64.35 ms (b) 64.51 ms (c) 64.90 ms (d) 65.07 ms

Figure 3. Bubble coalescence under symmetric BC of left and right faces. The color bar, *Scr2*, is the bubble ID and its maximum value denotes the total number of bubbles. $Scr2 = 2$ in (a) because the departed bubbles are still so close to the remaining bubbles that bubble IDs have not updated yet.

3.1.3. Periodic BC

The simulation with periodic BC was more numerically challenging. The two vents on the left and right surfaces (the left vent marked by the red box in Figure 4: left face 216, rotated horizontally to conserve space) were assigned with opposite velocities; therefore, applying periodic BC contradicts the velocity directions. To increase the stability of the simulation, the left/right surface was split into two portions by the black line marked in Figure 4. The top portion was still the non-slip wall BC, which is the same as that given in Li et al. [5]. However, the bottom portion was assigned with periodic BC. Considering that the bubble motions all happened at the bottom part of the domain, the wall BC on the top had a negligible effect on bubble interactions. Therefore, the domain could be treated with periodic BC on all four side faces (front and back, left and right). The split surface prevented the mesh size and computational cost from increasing significantly.

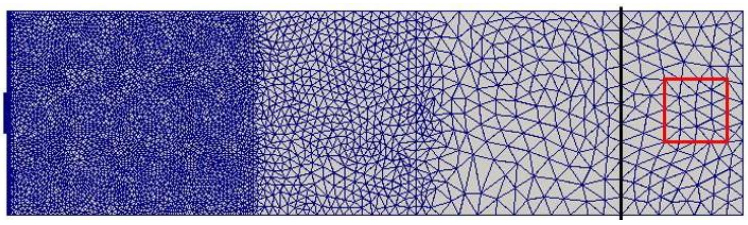

Figure 4. Illustration of splitting boundary faces (Left face 216, rotated horizontally)

Figure 5 shows how the bubbles grew, departed, and then coalesced with each other. The bubble sizes increased as a result of the surrounding liquid being overheated by the bottom surface and turned into vapor. As the bubbles grew, the surface tension force holding the bubble shape was reduced. When the buoyancy force exceeded the surface tension force, the bubbles departed and left the remaining vapor in the cavity to continue growing. Afterwards, the two departed bubbles coalesced with each other and formed a large, flat bubble. If the heat flux of the bottom surface increased until reaching critical heat flux (CHF), then the coalesced bubble could have expanded into a gas film and could have blocked the liquid from cooling the heated surface.

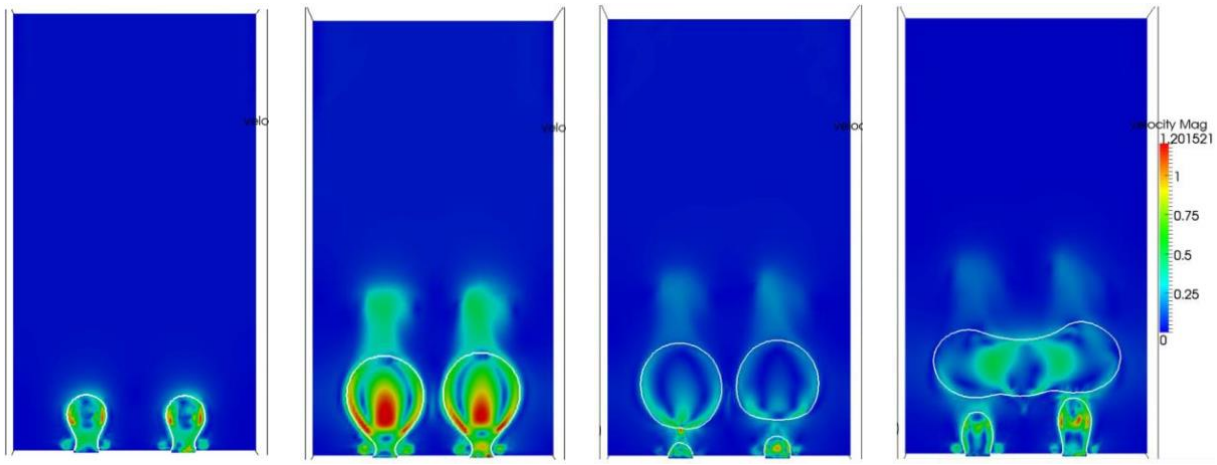

(a) 9.31 ms (b) 52.61 ms (c) 60.46 ms (d) 68.44 ms

Figure 5. Bubble topology change under periodic BC of left and right faces

3.1.4. Analysis of BC effect

To analyze bubble departure behavior, the growth of the equivalent radius for each BC was plotted as shown in Figure 6. Table II summarizes the departure time of each bubble under wall, symmetric, and periodic BCs individually. It is obvious that bubble departures under periodic BC were slightly promoted. As shown in Figure 2 (c), more periodic bubbles were involved in the boiling process. The closest distance from the periodic bubble to the original nucleation site was $S = 6\,mm$. Bubble departure diameter was D_d = 3.433mm, S/D_d = 1.75,which indicates an inhibitive effect of the bubble growth. However, the bubble departed slightly earlier. In addition, as Table II shows, left and right bubble departures did not necessarily occur at the same time, considering the complicated interactions between the bubble and the liquid, as well as the interactions between bubbles. The subtle difference of local fluid mechanics and temperature distributions around the bubble can all increase the interface instability, which yields different departure behaviors.

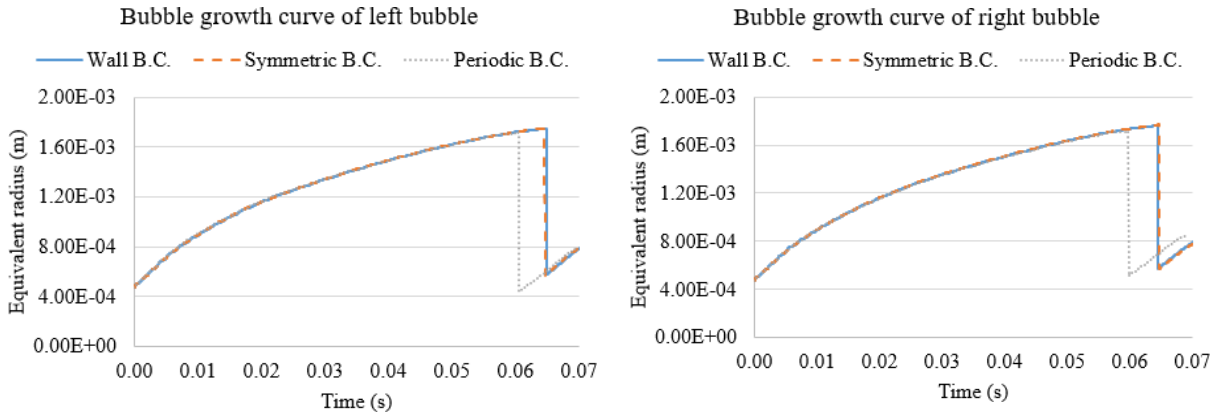

(a) Equivalent radius of left bubble (b) Equivalent radius of right bubble

Figure 6. Bubble growth curve under different BCs

Table II. Bubble Departure Behavior Comparison.

Departure	**Reference case (wall BC)**	**Symmetric BC**	**Periodic BC**
Left bubble departure time	64.85 ms	64.52 ms	60.46 ms
Right bubble departure time	64.42 ms	64.70 ms	59.81 ms
Left bubble departure diameter	3.501 mm	3.492 mm	3.437 mm
Right bubble departure diameter	3.528 mm	3.530 mm	3.433 mm

3.2. Pool Boiling with Four Active Nucleation Sites

This study was designed as a scale test, with a larger domain having nine nucleation sites, of which four were activated. Compared with the two-nucleation site problem, the size of the geometry and the number of elements were both significantly increased. This test was necessary to demonstrate the solver's capability to perform large-scale simulations.

3.2.1. Simulation setup

Figure 7 (a) depicts the domain with nine nucleation sites. The three edges of the cubic domain are all 18 mm. At the bottom surface, the distance along x or z directions between each two nucleation sites is 6 mm. This is different from the two-bubble boiling simulations (4 mm) in Section 3.1, which induces bubble coalescence to occur shortly after bubble departure. As a comparison, a distance of 6 mm allowed more interactions among bubbles. Although the distance among sites changed, the sizes of each cavity and each bubble as well as the initial temperature field remained the same. Another change in computational domain was the shape of the vents. The vents extend in x direction to guarantee no backflow on the top outlet, considering that the domain was expanded from 5 to 18 mm in the x direction. Similar to the periodic BC settings in two-bubble simulations, the two faces around the vents were also split into an upper non-slip wall portion and a lower periodic BC portion.

Figure 7 (b) shows the mesh on the bottom surface resolved by prism boundary layer mesh, and tetrahedral mesh was used elsewhere. Since five nucleation sites were deactivated, only the regions around 4-bubbles needed to be refined. To carefully resolve the vicinity of the bubble and minimize the computational cost, several cylindrical refinement regions were assigned around the bubble, as shown in Figure 7 (c)(d). The

diameter of each refinement cylinder was set slightly larger than the bubble departure diameter in Table II. There were 21 elements across the bubble diameter, and the total mesh size was 6.3 M. It took approximately 6,400 core-hours on the local HPC, *Insight*, to produce the first bubble departure. The simulation with 9 nucleation sites all activated was successfully conducted on *Insight* as well with the number of mesh elements increased to 13 M. Due to the computational resource limitation, only the bubble growth was observed. Under such large mesh size, it was too expensive to continue the simulation until the bubble departure. Therefore, a more affordable setup (4 nucleation site domain with the same site distance 6 mm) is presented in the next section to discuss the bubble departure behavior.

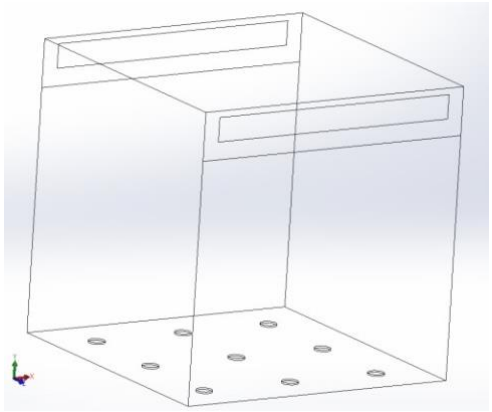

(a) Computational domain of 9 nucleation sites

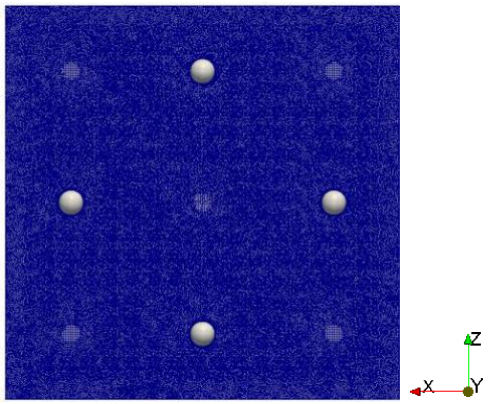

(b) 4 active nucleation sites (mesh at $y = 0.1mm$ plane)

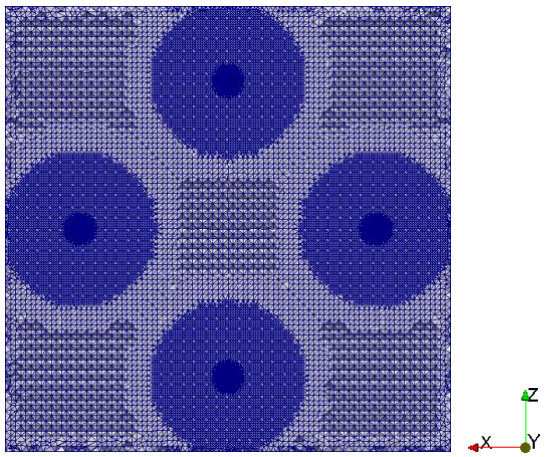

(c) 4 refined regions (mesh at $y = 0.6mm$ plane)

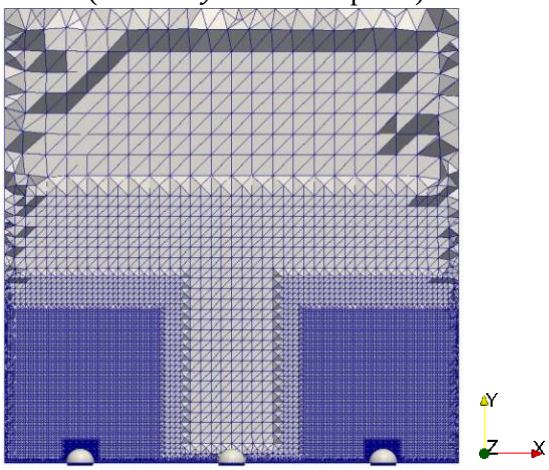

(d) Refined mesh across x-O-y plane

Figure 7. Mesh design of 4-bubbles distributed across 9 nucleation sites

3.2.2. Results of 9 nucleation sites boiling with 4 activated

Four-bubble departures are depicted in Figure 8 (a). With the new 4-bubbles in the domain, the corresponding bubble IDs are still recognized correctly, as Figure 8 (b) shows. Figure 8 (c) illustrates the temperature distribution of an $x - O - y$ plane across the center of the computation domain. The temperature distribution on the top of the departed bubble formed as a result of the pressure outlet BC applied on the top surface of the computation domain. The pressure was zero at the top of the domain, thus pressure reduced from the bottom to the dome of the bubble. Therefore, during the bubble growth, the liquid in the vicinity tended to move to the low-pressure region, and a temperature field formed with an upward trend.

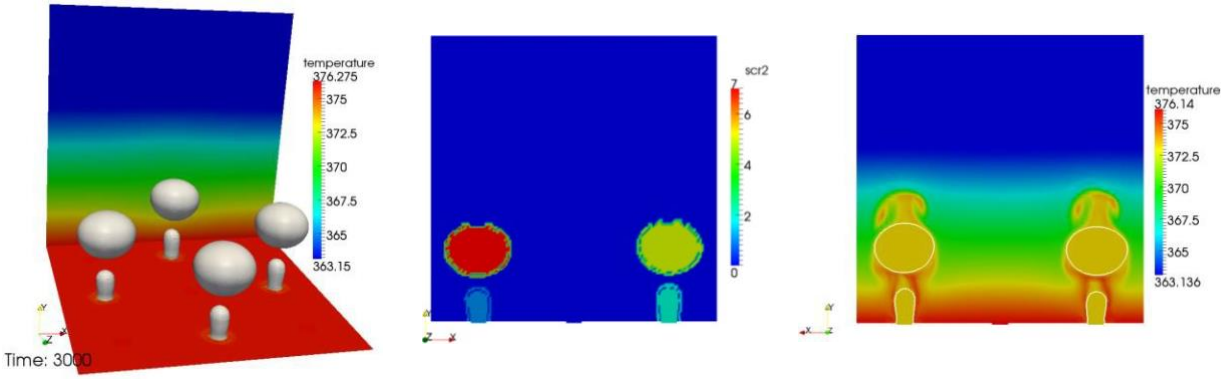

(a) Bubble departures on 9 nucleation sites with 4 activated

(b) Bubble identification

(c) Temperature distribution

Figure 8. Bubble departure for 4 active nucleation sites. The temperature units in color bars are all Kelvin (the same with the following figures).

3.2.3. Analysis of 9 nucleation sites boiling with 4 activated sites

The inactivated nucleation sites do not have an influence in the boiling process, so the current bubble distribution is sparse. The distance between each two activated nucleation sites on any axially aligned direction is $S = 12\ mm$, which is consistent with the base case of two-bubble boiling simulations [5]. In the base case, two bubbles existed inside a computation domain, with the wall BC on the two side faces and a nucleation site distance of $12mm$. However, the current case used periodic BC. Table III compares the bubble growth under different BCs. The two selected bubbles from the 4-bubble case were located on the $x - O - y$ plane. Because the simulation parameters were identical with those in Table I, the bubbles also departed at approximately the same time, 53.4 ms.

Table III. Comparison of 2- and 4-Bubble Simulations.

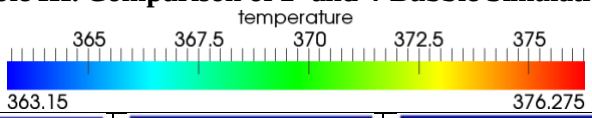

2-bubble with wall BC (adapted from Fig.3 of Li et al. [5], with permission)	$t = 10.5\ ms$	$t = 20.5\ ms$	$t = 31.5\ ms$	$t = 42.5\ ms$
4-bubble of 9 nucleation sites with periodic BC	$t = 10.69\ ms$	$t = 21.5\ ms$	$t = 31.82\ ms$	$t = 43.23\ ms$

For each comparison group, when the bubble shape and thermal boundary layer formations are similar to each other, then the computation time of the 4-bubble simulation is always slightly larger. As Figure 7 (b) shows, although the activated nucleation site distance was 12 mm (S = 12 mm, S/D_d = 3.41, independent region [4]), the distance between each simulation bubble and the nearby bubble on the 45 degree direction was $6\sqrt{2}$ mm (S = 6 mm, S/D_d = 2.49, inhibitive region [4]). Therefore, the bubble formation at one nucleation site inhibited the growth of the adjacent bubble on the 45-degree direction, so the 4-bubble simulation had a delay compared with the 2-bubble simulation, in which bubble interactions only occurred between those two nucleation sites.

3.3. Pool Boiling with Increasing Wall Heat Flux

The study of flow boiling at high heat flux directly contributed to model development for severe accident analysis of LWRs, but it is also important to develop, evaluate, and verify the boiling solver capabilities for no-flow (pool boiling) condition first. This section presents the heat flux effect on the boiling behavior. This is the first time that the boiling solver was tested on pool boiling with high heat fluxes, especially with multiple bubble growth. This is an essential step before reaching the critical heat flux condition.

3.3.1. Simulation setup

The geometry of the four-bubble nucleation sites under a square pattern was selected as shown in Figure 9 (a). The domain had a height of 18 mm and a cross section of 12 × 12 mm^2. At the bottom surface, the distance along x or z directions between each two nucleation sites was still 6 mm, the same as that
presented in Section 3.2. The size of each cavity also remained the same at 1 mm, and the bubble sizes were still 1.12 mm. The initial temperature field was also a linear function with $103°C$ at the bottom wall and $90°C$ at the top wall. The two faces around the vents were also split into the upper non-slip wall portion and the lower periodic BC portion, and all vertical faces surrounding the nucleation sites were periodic.

The mesh resolutions were similar to those presented in Section 3.1 and 3.2, and the same cylindrical refinement regions were used, as well, as shown in Figure 9 (b). There were 21 elements across the bubble diameter, and the total mesh size was 3.9 M. Three heat fluxes (q" = 50, 500, 5000 W/m^2) were applied
on the bottom wall to constantly heat the surface. It took approximately 2,048 core-hours on the local HPC, *Insight*, to produce the first bubble departure for q" = 5000 W/m^2. This number of core hours was even lower than the two-nucleation site boiling described in Section 3.1 because of the high heat flux. Bubble volume growth under high heat flux was incredibly fast, but the boiling model was still robust enough to handle such large phase changes.

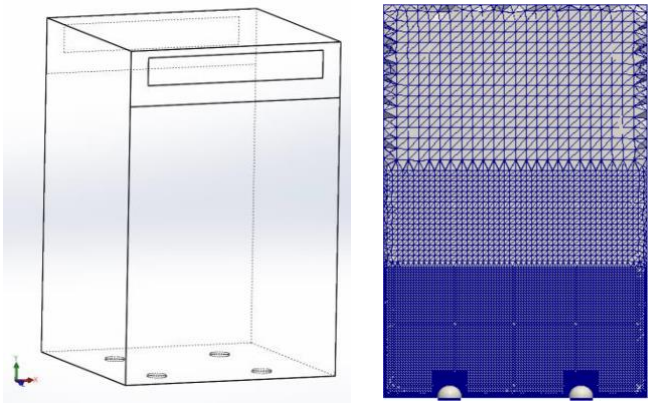

(a) Computational domain (b) Mesh design

Figure 9. Computational domain of 4 nucleation sites

3.3.2. Results of 4 nucleation sites

The simulation parameters were identical with those given in Table I, except that the q" was increased from 50 W/m^2 to 500 W/m^2 and then to 5,000 W/m^2 to study the changes of bubble interactions. Bubble departures occurred at different times, as Figure 10, Figure 11, and Figure 12 depict. According to the temperature color bar, the temperature near the bottom wall increased with heat flux, as expected.

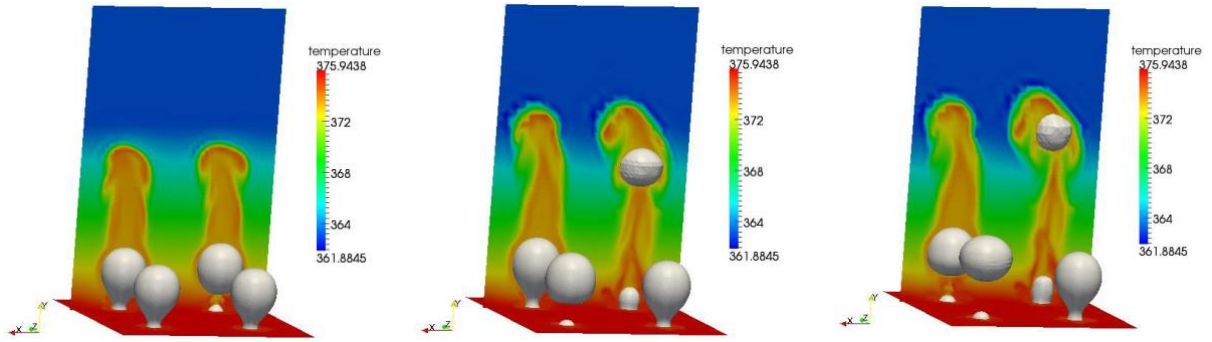

(a) 135.4 ms (b) 161.01 ms (c) 168.52 ms

Figure 10. Bubble departure in a time series under q" = 50 W/m^2

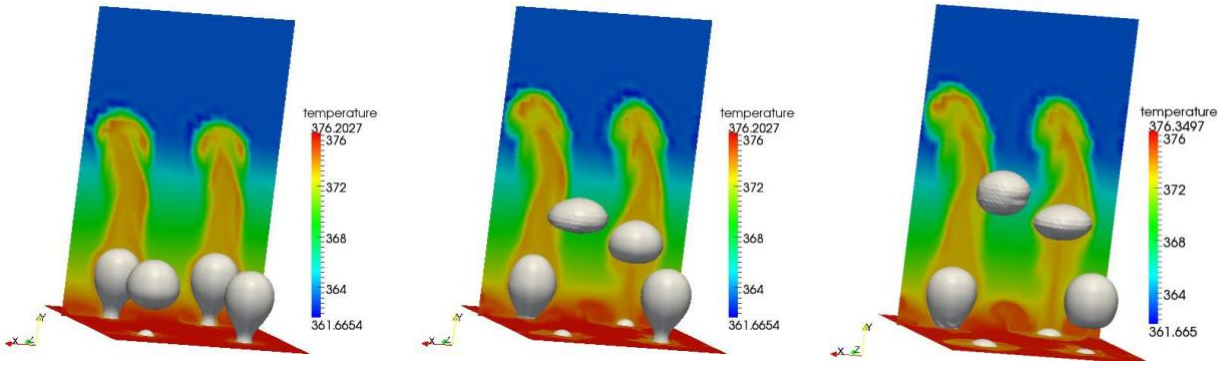

(a) 119.9 ms (b) 140.3 ms (c) 148.9 ms

Figure 11. Bubble departure in a time series under q" = 500 W/m^2

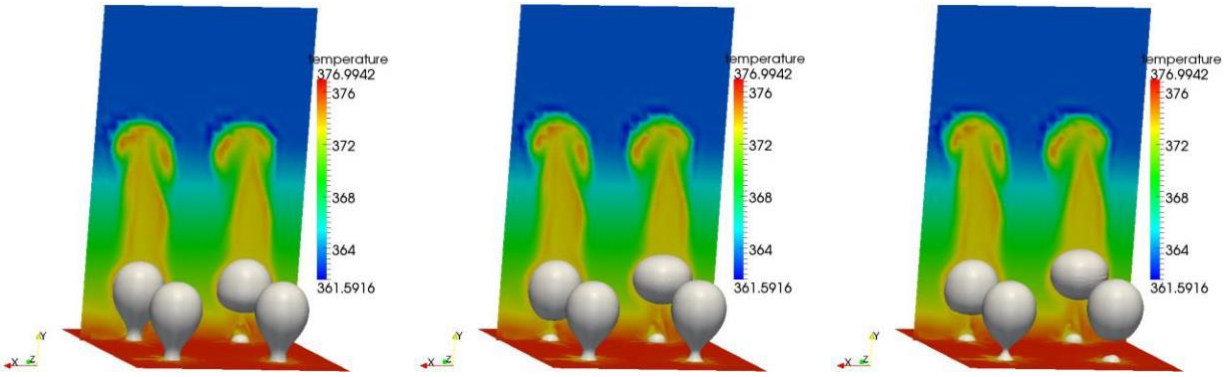

(a) 118.3 ms (b) 121.9 ms (c) 123.7 ms

Figure 12. Bubble departure in a time series under q" = 5000 W/m^2

3.3.3. Analysis of 4 nucleation sites

As Figure 10, Figure 11, and Figure 12 illustrate, the order of bubble departure changed under different heat fluxes. Figure 13 denotes the sequence with red numbers connected by arrows. The departure orders were the same under q" = 50 W/m^2 and q" = 500 W/m^2, but they were different under q" = 5000 W/m^2. Because the distance between each two-bubble on x or z direction (S = 6 mm) inhibited the growth of the nearby bubble, the furthest bubble (on the diagonal side, $S = 6\sqrt{2}\ mm$ away) should depart next. Such an interaction is observed for first to second bubble departure under low and medium heat flux (q" = 50 and 500 W/m^2), and second to third bubble departure under high heat flux (q" = 5000 W/m^2). Although for the high heat flux case, the second bubble departs is the bubble adjacent, rather than diagonal,
from Figure 12 (b)(c) it is clear the adjacent and the diagonal bubbles formed and departed almost at the same pace. High heat flux intensifies the bubble growth rate, and thus also disturbs the order of bubble departure.

Figure 10, Figure 11, and Figure 12 also qualitatively show that the departure frequency and diameter vary under different heat fluxes. Table IV summarizes the departure time and diameter for the first three bubbles. As heat flux increased, a decrease in the departure time (from 138.5 ms to 118.8 ms) and an increase in D_d (from 2.92 mm to 3.06 mm) can be observed for the first bubble. This phenomenon is expected because bubble growth rate is faster under higher heat flux.

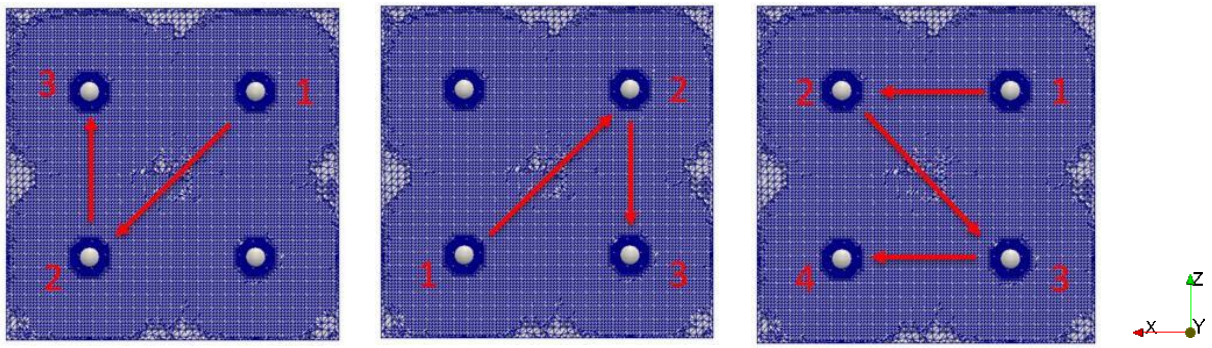

(a) q" = 50 W/m^2 (b) q" = 500 W/m^2 (c) q" = 5000 W/m^2

Figure 13. Bubble departure order under different heat fluxes. The sequences in (a) and (b) are essentially the same.

Table IV. Departure Time and Diameter for Pool Boiling with Increasing Heat Fluxes.

Departure time (ms)				**Departure diameter, D_d (mm)**			
q"(W/m^2)	50	500	5000	q"(W/m^2)	50	500	5000
1st bubble	138.5	117.0	118.8	1st bubble	2.92	3.02	3.06
2nd bubble	159.9	129.7	122.0	2nd bubble	3.06	3.05	3.06
3rd bubble	165.8	151.3	124.8	3rd bubble	3.10	3.07	3.05

As shown in Table IV, it is also clear that the departure time interval between the first and second bubbles reduces as heat flux increases. This time interval and the corresponding frequency are computed in Table V and plotted in Figure 14 with heat flux. The departure frequency is almost linearly proportional with the heat flux. Such behavior is reasonable because the bubble volume change is linearly proportional with heat flux. With more samples, the relationship between departure frequency and heat flux can be further

explored. It is worth mentioning that the departure frequency shown here differs from the formal definition of bubble departure frequency. The former is the departure frequency in which two bubbles depart

sequentially after one another from multiple nucleation sites, but the latter corresponds to the frequency at which bubbles depart from the same nucleation site for multiple boiling cycles.

Table V. Departure Time Interval and Frequency between First and Second Bubbles.

$q''(W/m^2)$	50	500	5,000
Departure time interval	21.4	12.7	3.2
Frequency	0.0467	0.0787	0.3125

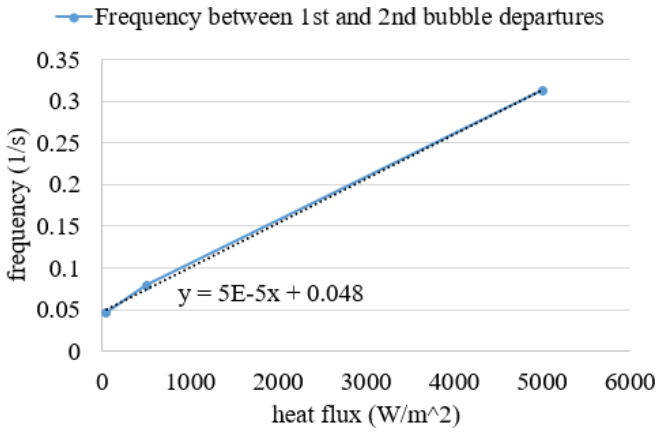

Figure 14. Bubble departure frequency under different heat fluxes

3.4. Comparison of boiling behavior under different nucleation site patterns

The simulations presented in Section 3.1.3, Section 3.2, and Section 3.3 all include pool boiling simulations under heat flux 50 W/m^2 and periodic BC setup. The first bubble departure times of those three simulations are compared in Table VI. For the 2-site 2-bubble condition, $S/D_d \in (1,3)$; thus bubble growths inhibit each other. It is expected that the 9-site 4-bubble condition has a smaller departure time, considering $S/D_d > 3$; thus bubble growths are independent of each other. However, the departure time of the 4-site 4-bubble condition is much longer. It is possible that the first bubble is not only inhibited by the other bubble on the same $x - O - y$ plane, but it also may be suppressed by the remaining two bubbles since the nucleation sites are either $6mm$ or $6\sqrt{2}\ mm$ away, so S/D_d all belong to inhibitive regions. Inhibitive effects from three directions are superimposed on the first bubble, which extensively delays the departure. Such a superimposed inhibitive effect was not discussed in previously published works to the best of the authors' knowledge. Further studies are needed to verify this observation and to explore the quantitative relationship between bubble departure behavior and nucleation site patterns.

Table VI. First Bubble Departure Time Comparison under q'' = $50W/m^2$ and Periodic BC.

Section	Nucleation site pattern	S (mm)	D_d (mm)	S/D_d	First bubble departure time (ms)
3.1.3	2-site 2-bubble	4	3.433	1.165	59.81
3.2	9-site 4-bubble	12	3.407	3.522	53.4
3.3	4-site 4-bubble	6	2.92	2.055	138.5

4. CONCLUSIONS

High-fidelity pool boiling simulations can provide a numerical database for improving mechanistic boiling models by specifically evaluating the interactions among bubbles. Previously published pool boiling simulations studied two nucleation sites in which bubble growth at one site suppressed the nucleation at the other site. However, when more nucleation sites were involved, the complexity of bubble suppression from surrounding sites increased, as well.

To improve the understanding of bubble departure behavior, additional interface capturing simulations were conducted on pool boiling scenarios with multiple nucleation sites. A boiling model in PHASTA was used for all presented simulations incorporating the level-set method. Such interface-capturing boiling simulations are computationally expensive, especially when resolved by uniform fine meshes. The presented simulations used unstructured meshes in PHASTA with local refinements, which greatly reduced the computational cost but still maintained the accuracy of regions of interest.

In the first study, different BCs were used to assess the robustness and reproducibility of the boiling solver. Symmetric BC produces almost identical coalescence time compared with that under wall BC [5], which strengthens the reproducibility of the solver. Periodic BC is more numerically challenging considering opposite velocities of the two vents on the left and right faces. However, the boiling solver was still robust enough to show bubble growth, departure, and coalescence. Under periodic BC, bubble departures were slightly promoted due to the subtle difference of local fluid mechanics and temperature distributions induced by periodic bubbles.

In the second study, a larger domain with 9 nucleation sites, 4 of which were activated, was investigated. Although the axially aligned nucleation site distance (S = 12 mm) was consistent with the "base case" in two-bubble boiling simulations [5], the bubble departure was relatively delayed. The nearby bubbles on the 45-degree directions were found to inhibit the growth of the adjacent bubble.

The third parametric study was performed to investigate bubble departure behavior influenced by wall heat flux. With the increase of heat flux, the order of bubble departure became different, but two bubbles on the diagonal side always departed sequentially after one another. The departure time interval between the first and second bubbles reduced as the heat flux increased. The corresponding frequency was almost linearly proportional with the heat flux. In addition, multiple nucleation sites with a dense nucleation site pattern extensively delayed the first bubble departure under superimposed inhibitive effects from nearby bubbles.

The presented work provides new insight on the fundamental understanding of boiling phenomenon, contributes to the development of the 3D M-CFD model, and provides a more comprehensive database for data-driven pool boiling studies. The studies outlined above also fill a critical gap in capability development and demonstration. For future work, model validation can be performed by comparing the numerical bubble topology with high-resolution pool boiling and flow boiling experiments, and the effect of nucleation site pattern on bubble departure behaviors can be explored further.

ACKNOWLEDGMENTS

This research is supported by the Consortium for Advanced Simulation of Light Water Reactors (http://www.casl.gov), an Energy Innovation Hub (http://www.energy.gov/hubs) for Modeling and Simulation of Nuclear Reactors under the US Department of Energy [grant number DE-AC05-00OR22725]. The solution presented here uses Acusim linear algebra solution library provided by Altair Engineering Inc. and meshing and geometric modeling libraries by Simmetrix, Inc.

REFERENCES

1. L. ZHANG and M. SHOJI, "Nucleation site interaction in pool boiling on the artificial surface," *Int. J. Heat Mass Transfer,* **46**, 513-522 (2003).

2. R. MALLOZZI, R.L. JUDD, N. BALAKRISHNAN, "Investigation of randomness, overlap and the interaction of bubbles forming at adjacent nucleation sites in pool boiling," *Int. J. Heat Mass Transfer,* **43**, 3317-3330 (2000).

3. C. HUTTER, K. SEFIANE, T. KARAYIANNIS, A. WALTON, R. NELSON, D. KENNING, "Nucleation site interaction between artificial cavities during nucleate pool boiling on silicon with integrated micro-heater and temperature micro-sensors," *Int. J. Heat Mass Transfer,* **55**, 2769-2778 (2012).

4. V. CHEKANOV, "Interaction of centers in nucleate boiling," *High Temperature Science,* **15**, 121-128 (1977).

5. M. LI, J. MOORTGAT, I.A. BOLOTNOV, "Nucleate boiling simulation using interface tracking method," *Nucl. Eng. Des.,* **369**, 110813 (2020).

6. M. LI and I.A. BOLOTNOV, "The evaporation and condensation model with interface tracking," *Int. J. Heat Mass Transfer,* **150**, 119256 (2020).

7. K.E. JANSEN, "A stabilized finite element method for computing turbulence," *Comput. Methods Appl. Mech. Eng.,* **174**, 299-317 (1999).

8. K.E. JANSEN, "Unstructured grid large eddy simulations of wall bounded flows," *Annual Research Briefs, Center for Turbulence Research, NASA Ames/Stanford University,* , 151 (1993).

9. J. FENG and I.A. BOLOTNOV, "Interfacial forces evaluation on a single bubble in shear flows using interface tracking approach". *Transactions of the American Nuclear Society*, Washington, D.C., November 8-12113, 1512-1514 (2015).

10. J. FANG, M. RASQUIN, I.A. BOLOTNOV, "Interface tracking simulations of bubbly flows in PWR relevant geometries," *Nucl. Eng. Des.,* **312**, 205-213 (2017).

11. M. LI, K. ZENG, L. WONNELL, I.A. BOLOTNOV, "Development of a New Contact Angle Control Algorithm for Level-Set Method," *Journal of Fluids Engineering,* **141**, 061301 (2019).

12. M. SUSSMAN, A.S. ALMGREN, J.B. BELL, P. COLELLA, L.H. HOWELL, M.L. WELCOME, "An adaptive level set approach for incompressible two-phase flows," *Journal of Computational Physics,* **148**, 81-124 (1999).

13. SETHIAN, A.J., 1999. Level Set Methods and Fast Marching Methods. Cambridge University Press.

14. S. NAGRATH, K.E. JANSEN, R.T. LAHEY, "Computation of incompressible bubble dynamics with a stabilized finite element level set method," *Comput. Methods Appl. Mech. Eng.,* **194**, 4565-4587 (2005).

15. N. BASU, G.R. WARRIER, V.K. DHIR, "Onset of nucleate boiling and active nucleation site density during subcooled flow boiling," *TRANSACTIONS-AMERICAN SOCIETY OF MECHANICAL ENGINEERS JOURNAL OF HEAT TRANSFER,* **124**, 717-728 (2002).